Manuscript prepared for Ann. Geophys.
with version 2015/04/24 7.83 Copernicus papers of the LaTeX class copernicus.cls.
Date: 27 October 2015

Simultaneous observations of structure function of refractive index using a high resolution radar and the DataHawk small airborne measurement system

Danny E. Scipión[1], Dale A. Lawrence[2], Ronald F. Woodman[3], Diego A. Lume[1], Marco A. Milla[1], and †Ben B. Balsley[4]

[1]Radio Observatorio de Jicamarca, Instituto Geofísico del Perú, Lima, Peru
[2]Aerospace Engineering Sciences, University of Colorado, Boulder, CO, USA
[3]Instituto Geofísico del Perú, Lima, Peru
[4]Cooperative Institute for Research in Environment Sciences, University of Colorado, Boulder, CO, USA

Correspondence to: Danny E. Scipión (danny.scipion@jro.igp.gob.pe)

Abstract. The SOUSY (SOUnding SYstem) radar was relocated to the Jicamarca Radio Observatory (JRO), near Lima, Peru in 2000, where the radar controller and acquisition system were upgraded to state-of-the-art parts to take full advantage of its potential for high-resolution atmospheric sounding. Due to its broad bandwidth (4 MHz), it is able to characterize clear-air backscattering with high spatial resolution (37.5 m).

A campaign conducted at JRO during July 2014 aimed to characterize the lower troposphere with a high temporal resolution (8.1 Hz) using the DataHawk (DH) small unmanned aircraft system, which provides in-situ atmospheric measurements at scales as small as 1 m in the lower troposphere, and can be GPS-guided to sample within the beam of the radar. This was a unique opportunity to make coincident observations by both systems, and to directly compare their in-situ and remotely sensed parameters.

Because SOUSY only points vertically, it was only possible to directly retrieve changes in the refractive index as a function of height through the structure function of refractive index C_n^2. Calculations of C_n^2 from the DH are obtained by combining pressure, temperature, and relative humidity measurements at the radar resolution. C_n^2 from the radar is estimated using Bragg scattering theory. Excellent agreement is observed between the C_n^2 estimates obtained from the DH and SOUSY in the overlapping measurement regime from 1000 m up to 3500 m above ground, and this correspondence provides the first accurate calibration of the SOUSY radar for measuring C_n^2.

1 Introduction

Radars have proven to be important tools for investigating dynamic processes of different temporal and spatial scales in the lower and middle atmosphere (e.g. Woodman and Guillen, 1974; Rüster

et al., 1986; Luce et al., 2002, 2007). Frequencies ranging from MF (Medium Frequency - 3 MHz) to UHF (Ultra High Frequency - 3 GHz) are the most common for studying dynamic processes and structures in the neutral atmosphere.

In general, VHF (Very High Frequency) and UHF stratosphere-troposphere (ST) clear-air radar returns are sensitive to electromagnetic refractive index fluctuations, which depend primarily on fluctuations in temperature (T) and humidity (RH) at half the radar wavelength, but not directly on the mechanical turbulence in an air parcel and the associated velocity fluctuations (Luce et al., 2002). Moreover, radar returns can be due to isotropic fluctuations in T and RH associated with active turbulent mixing, or from anisotropic sheets of stable stratification at the edges of mixing layers. Coupled with typical radar vertical resolutions (100 - 200 m) that are large compared to the vertical scales of these disparate phenomena, it has been difficult to infer what phenomena the radar returns represent.

Additional measurements are clearly needed, both at higher resolution and with complementary sensitivities to the phenomena of interest. Recent work has compared the backscatter echo received by radar (at 50 m resolution and corrected for range attenuation effects) with the square of the mean vertical gradient of the generalized potential refractive index (obtained from high-resolution radiosonde balloons) Luce et al. (2002, 2007) and references therein. These have produced excellent correspondence under particular atmospheric conditions with persistent horizontal structure, where the large (many km) separation between an advected balloon and the radar beam are inconsequential. In the present work, we describe significant improvements in measurement resolution and coincidence between VHF radar returns and in-situ measurements in the lower troposphere.

The SOUSY (SOUnding SYstem) VHF radar is a powerful tool to study mainly the troposphere and stratosphere (Rüster et al., 1986), and its observations include wind fields, frontal zones and tropopause height, cumulus convection, gravity waves source mechanism, and jet stream-generated dynamic instabilities and turbulence. After its installation at the Jicamarca Radio Observatory (JRO), there have been two main modifications to the SOUSY system (Woodman et al., 2003): first, the antenna size and shape were modified to enable two fixed-beam pointing directions and second, the control and data acquisition modules were upgraded with a digital receiver system to take full advantage of the wide power-stage bandwidth (4 MHz), resulting in a high spatial resolution (37.5 m).

Coincident in-situ measurements of the atmosphere were obtained using a small unmanned aircraft system (sUAS) developed at the University of Colorado, called the DataHawk (Lawrence and Balsley, 2013). This system consists of a GPS-controlled, battery-operated aircraft (1 m wingspan), programmed to fly 100 m diameter circles ascending or descending entirely in the radar beam, while measuring temperature, humidity, and winds at high vertical resolution ($\sim$1 m). Through post-processing of this data, it can also measure ϵ (turbulent energy dissipation rate), and structure functions C_T^2 (temperature), C_H^2 (humidity), and as used here, C_n^2 (refractive index) (Balsley et al., 2012). In order to reach the altitudes above the 1 km radar ground clutter, the DataHawk

was dropped from a conventional weather balloon, and flown under permission from The Peruvian Corporation of Commercial Airports and Aviation Inc. (CORPAC) air traffic control.

The present work describes the results of this unique coordinated observational campaign where the DH flies on a tight spiral up and down the high resolution SOUSY radar antenna beam over an altitude overlap range of 1 - 3.7 km. This provides the first comparisons using 8.1 Hz co-located in-situ measurements of pressure, humidity, and temperature acquired with the DH and scaled to the 37.5 m SOUSY radar resolution. The paper is structured as follows: Sect. 2 describes the theoretical basis for estimating C_n^2 from both in-situ DH and radar backscatter measurements. Sect. 3 provides details on the experimental setup. In Sect. 4, the data collection is described along with the C_n^2 comparison results. Finally, In Sect. 5, conclusions and future work are outlined.

2 Theoretical background

In-situ and remotely sensed observations are compared on the basis of the structure parameter of refractive index C_n^2 that is briefly reviewed here. Its estimation from the DH and SOUSY instruments is discussed in separate subsections below.

The energy spectrum of turbulence $E(\kappa)$ proposed by Kolmogorov can be classified into three regions (Pope, 2000): the energy-containing range, the inertial subrange, and the dissipation range. Under this hypothesis (White, 1997), there is no exchange of energy between the energy-containing range and the dissipation range. Instead, the rate of energy transfer from large scales in the energy-containing range is equivalent to the energy dissipation rate at small scales in the dissipation range. In the inertial subrange, the bulk of energy transfers from larger to smaller scales following a wavenumber slope of -5/3. This is also known as *energy cascade* assumption or *Kolmogorov -5/3 turbulence spectrum* for isotropic turbulence, where the turbulence has the same variance in all directions (Stull, 2000).

Under these conditions the energy spectrum of turbulence per unit mass $E(\kappa)$ can be expressed as:

$$E(\kappa) = A_e \epsilon^{2/3} \kappa^{-5/3}, \tag{1}$$

where A_e is a universal dimensionless constant between 1.53 and 1.68 (Gossard and Strauch, 1983) and $\kappa = 2\pi/\lambda$ represents the wavenumber. In the troposphere inertial subrange, typically spans large eddy scales of 200 m down to small eddy sizes of 1 cm (Wallace and Hobbs, 2006).

Considering that these turbulent eddies contain air parcels with variations in temperature and humidity, hence also in the refractive index n, and assuming that the turbulence is both isotropic and in the inertial subrange, C_n^2 ($\mathrm{m}^{-2/3}$) parameterizes the refractive index structure function D_n as follows (Tatarskii, 1971):

$$D_n(\boldsymbol{\delta}) = \left\langle [n(\mathbf{r}+\boldsymbol{\delta}) - n(\mathbf{r})]^2 \right\rangle, \quad (2)$$

$$D_n(\delta) = C_n^2(r)\delta^{2/3}, \quad (3)$$

$$C_n^2 = \frac{\left\langle [n(\mathbf{r}+\boldsymbol{\delta}) - n(\mathbf{r})]^2 \right\rangle}{|\boldsymbol{\delta}|^{2/3}}, \quad (4)$$

where $< \cdot >$ denotes the spatial average over a volume within which the n irregularities are assumed to be statistically isotropic and homogeneous. Here, $\mathbf{r}$ represents the position vector, $\boldsymbol{\delta}$ denotes the spatial separation over which the structure function is being computed (vertical here), and $\delta = |\boldsymbol{\delta}|$.

2.0.1 In-situ DH Measurement of C_n^2

If the background atmospheric pressure profile is in hydrostatic balance, then the refractivity $N = (n-1) \times 10^6$ can be found directly from the following equations of state (Bean and Dutton, 1966; Rogers and Yau, 1989; Holton, 2004):

$$\mathrm{d}\ln P = -\frac{g}{RT}\mathrm{d}z, \quad (5)$$

$$e_s = 6.112 \exp\left(\frac{17.6T}{T+243.5}\right), \quad (6)$$

$$e = \frac{fe_s}{100}, \quad (7)$$

$$N = \frac{77.6}{T+273.11}\left(P + \frac{4811e}{T+273.11}\right), \quad (8)$$

where P is total atmospheric pressure (hPa), e_s is the saturated vapor pressure (hPa), f is the relative humidity (%), e is the partial pressure of water vapor (hPa), P_0 represents the pressure at z = 0 m (1000 hPa), g is the gravitational acceleration (9.81 m s^{-2}), R is the gas constant for dry air (287 J kg^{-1} K^{-1}), and T is the temperature (°C). The electron density term has been omitted in Equation (8) due to its influence only in the ionosphere.

The DH provides in-situ measurements of P, e, and T at 8.1Hz. With a vertical ascent/descent rate of 2.0 m s^{-1}, refractivity N (or equivalently refractive index n) can be estimated with a vertical resolution of 0.25 m. Assuming that turbulence is isotropic and in the inertial subrange (verified in Section 4), the structure function for any desired $\delta > 0.25$ m can be estimated by calculating C_n^2 via Equation (4). For comparisons with the SOUSY radar, C_n^2 estimations from the DH must be at the radar Bragg scale $\delta = \sim$2.8 m @ 53.5 MHz, (Scipión et al., 2008). This is computed from the C_n^2 estimates at the DH sampling scale as follows:

$$C_n^2 = \frac{(\Delta n)^2}{\delta^{2/3}} \quad (9)$$

where Δn represents the refractive index difference over the Bragg scale δ.

2.0.2 SOUSY Radar Measurement of C_n^2

Radars transmit pulses at a high power in order to maintain the required sensitivity to detect reflections from weak targets at a desired maximum range. The *radar equation* is used to determine the returned power P_r based on multiple parameters from a single target with backscattered cross-section σ_b (Skolnik, 1990; Doviak and Zrnić, 1993).

$$P_r = \frac{P_{avg} G^2 \lambda^2 \sigma_b f^4(\theta, \phi)}{(4\pi)^3 r^4 l^2}, \tag{10}$$

where P_{avg} is the averaged transmitted power, G^2 represents the gain of the transmitting and receiving antennas for the monostatic case, and λ is the radar wavelength. The range to the target is represented by r, l represents the attenuation losses, and $f^4(\theta, \phi)$ is the two-way normalized power density pattern. The radar equation for a volume filled with targets (Doviak and Zrnić, 1993; Cohn, 1995; Hocking, 1985, 1996; White, 1997) that is used for atmospheric scatters can be presented as:

$$P_r = \frac{P_t d G^2 \lambda^2}{(4\pi)^3 r_0^2 l^2} \times \frac{c\tau_w}{2} \times \frac{\pi \theta_1^2}{8 \ln 2} \times \eta, \tag{11}$$

where $P_{avg} = P_t \times d$, P_t is the peak transmitted power, d is the duty cycle, and r_0 is the range to the center of the resolution volume. The radar resolution volume refers to the minimum separation between two volume targets that permits them to be distinguished by a radar. The second term on the right-hand-side of the equation represents the range resolution $\Delta r = c\tau_w/2$, where τ_w is the transmitting pulse width. The third term on the right-hand-side represents the transmitting beamwidth, where θ_1 is the 3-dB width (in radians) of the one-way pattern (Doviak and Zrnić, 1993). Finally, the radar reflectivity η, or average backscatter cross-section per unit volume (White, 1997), is a measurement of the radar scattering intensity in units of m^{-1}.

The radar reflectivity for clear-air radars is a measurement of the intensity caused by refractive index fluctuations present in the radar resolution volume. If the radar half-wavelength (Bragg scale $\lambda_B = \lambda/2$) lies within the inertial subrange, the radar reflectivity can be represented as (Tatarskii, 1961; Ottersten, 1969; Cohn, 1995; Doviak and Zrnić, 1993; White, 1997):

$$\eta = 0.379 C_n^2 \lambda^{-1/3}. \tag{12}$$

The received radar power P_r is proportional to the radar reflectivity η, which is a measure of the radar scattering intensity (see Equation (11)). Also, η is proportional to C_n^2 (see Equation (12)). If the radar is calibrated, C_n^2 can be obtained by the above from measurements of return power at every radar dwell time (at the sampling resolution volume Δr =37.5 m).

Unfortunately, an accurate radar calibration can be complex, requiring detailed measurements of the various radar parameters (see Equation (11)), such as the transmitted peak power P_t, duty cycle d, antenna gain G, antenna efficiency, radar beamwidth θ_1, among others. After combining Equations (11) and (12), and grouping all the radar parameters that are hard to measure or quantify

in a calibration constant C, a simplified equation for the estimation of C_n^2 can be expressed as:

$$\log C_n^2 = \log(P_r \times r_0^2) - \log d - \log \tau_w + C, \tag{13}$$

where $P_r \times r_0^2$ represents the total range-corrected power.

Estimates of C_n^2 from the DH and the SOUSY radar have been calculated at two different scales, Bragg scale (2.8 m) and radar range resolution (37.5 m) respectively. From radar theory, the received power is due to the contribution of all eddies weighted in range (Muschinski et al., 1999; Scipión et al., 2008). A similar analogy can be applied to the C_n^2 estimates obtained from the DH for fair comparison between the two instruments:

$$C_n^2 = \frac{1}{M} \sum_{m=1}^{M} C_n^{2(m)} \times W_r^{(m)}, \tag{14}$$

where m indexes the contribution of each individual eddy of the total of M DH's eddies within the resolution volume centered at the range r_0. The range weighting function W_r represents the convolution between the impulse response of the receiver with the transmitted pulse and is described by (Holdsworth and Reid, 1995; Scipión et al., 2008) as:

$$W_r^{(m)} = \exp\left[-\frac{(r^{(m)} - r_0)^2}{2\sigma_r^2}\right], \tag{15}$$

where $r^{(m)}$ represents range of the m eddy and the variance is $\sigma_r = 0.35 c\tau_w/2$.

3 Experimental setup

3.1 Site description

The SOUSY radar is installed at the Jicamarca Radio Observatory (JRO), located at 511 m above sea level approximately 25 km from the city of Lima, Peru. The location of the DataHawk launch site is approximately at 0.8 km North-East from the SOUSY radar because it is both close to the radar site and far away from possible sources of interference during calibration. See FIG. 1.

3.2 SOUSY radar

The SOUSY radar was donated by the Max Planck Institut für Aeronomie to the Instituto Geofísico del Perú in 2000 (Woodman et al., 2003) and installed at JRO to complement JRO studies due to SOUSY's large bandwidth (4 MHz compared to 700 kHz from the Jicamarca radar) which provides atmospheric measurements with high spatial resolution (37.5 m). SOUSY specifications and parameters are presented in Table 1.

Shortly after its installation at Jicamarca, a new digital acquisition system was developed using an off-the-shelf AD6620 digital receiver board to take full advantage of SOUSY's large power-bandwidth (Woodman et al., 2003; Alcantara and Abad, 2008). For the upgrade to be fully functional, it included a radar controller and direct digital synthetizer.

Initial results confirmed SOUSY's ability to provide high range-resolution, which proves that it is a valuable tool to study the morphology of turbulent layers under statistically stable stratified conditions (Woodman et al., 2007). During the present campaign the beam was set to point vertically, to be coincident with vertical DataHawk helix profiles.

3.3 DataHawk

The DataHawk is a sUAS that was specifically designed for high-resolution, multiple-variable, state-of-the-art atmospheric sensing measurements (Lawrence and Balsley, 2013). The atmospheric regions target by the DataHawk are the Atmospheric Boundary Layer (ABL), and lower troposphere (up to 10 km).

The maximum altitude reached by the DH depends on the launch method: when launched from the ground (bungee launch), it can reach up to 2.5 km at a 2 m s^{-1} rise rate. Higher altitudes (up to 10 km) can be reached when it is launched by a balloon drop (see FIG 2 a), in which the DH detaches at a prescribed altitude, then flies back upwind to the desired region (FIG. 2 b). Upon reaching the study region, the DH descends (or ascends depending on the launch method) in a helix trajectory as shown in FIG. 2 c. A detailed list of the capabilities, sensors, and system characteristics of the DataHawk is provided in Table 2.

4 Results

A campaign for coordinated observations using the DataHawk and the SOUSY radar was conducted between July 5 and 10, 2014. The first few days were used to setup the instruments, test the launch site, and conduct the test flights. The main observations were made on July 10, 2014. There were two flights that reached the desired altitude within the radar beam (see Table 3).

Two radar pulse configurations were tested with SOUSY and are outlined in Table 1. The main difference between the two modes is the average transmitted power: Mode 1 transmits eight times the power of Mode 2 and uses pulse compression to keep the same range resolution.

Radar returns for July 10, 2014 between 09:10 and 17:30 LT are presented in FIG. 3. Data between 9:10 - 13:50 were acquired using Mode 2, while data between 14:40 - 17:30 were acquired using Mode 1. The gap observed between 13:50 and 14:40 was due to an upgrade in the T/R switch. This upgrade gave a better recovery time of the signal, which allowed the detection of layers down to 500 m range, in comparison with the old design that only allowed discrimination of turbulent layers from ranges above 1.2 km. For better comparison of both modes, the power is corrected by range and the difference in the average transmitted power.

Many layers with good resolution can be clearly observed throughout the day, which shows SOUSY's potential for turbulence studies. Both DH flights over SOUSY are seen in the radar data as straight lines relating altitude and time, with an increase in the returned power (see the saturated

red lines between 11:05 and 11:30, and between 15:20 and 15:45). In addition to the increase in the returned power from DataHawk reflections, the vertical velocity signatures of the DH flights can be observed in FIG. 4. The evolution of the updrafts and downdrafts throughout the day and their propagation to altitudes up to 6.5 km can also be observed.

4.1 Results from 10.7.2014, flight starting at 10:03:46 LT

The morning flight over the SOUSY radar was a balloon drop using a tethered balloon that reached approximately 2 km from the launch site. Right after the drop, the DH flew over the SOUSY radar and started its spiral ascent up to 2.8 km, which was limited because of battery life. After reaching its maximum altitude, it descended down to 500 m and returned to the launch site for landing. The total time of the flight over SOUSY was approximately 25 mins. A close up of the calibrated range-corrected received power is presented in FIG. 5. The black line presented on top of the radar data represents the altitude measured directly by a pressure sensor on the DataHawk. Not only can the DH ascent and descent be clearly observed in the radar data, the agreement in time and altitude between these instruments is within the resolution of the data (37.5 m in altitude, 12.5 seconds in time).

A verification that the data are in the inertial subrange is performed by calculating the 1-dimensional refractive index spectra $S_n(\kappa)$, which should exhibit the form of the Kolmogorov -5/3 turbulence (Doviak and Zrnić, 1993):

$$S_n(\kappa) = \frac{\Gamma\left(\frac{5}{6}\right) C_n^2 \kappa^{-5/3}}{3 \times 2^{1/3} \Gamma\left(\frac{2}{3}\right) \sqrt{\pi}}, \tag{16}$$

where $\kappa = 2\pi/\lambda$ is the wavenumber. A practical way to calculate $S_n(\kappa) = S_n(k\Delta_\kappa)$ is to interpolate the DataHawk data, then re-sampling it at a fixed spatial grid of 0.25 m to resolve slight variations in vertical rate, then compute the fast Fourier transform (FFT) of the uniformly resampled DH data :

$$S_n(k\Delta_\kappa) = \frac{2\Delta_\lambda}{M} \left| \sum_{m=0}^{M-1} n(m\Delta_\lambda) e^{-j2\pi km/M} \right|^2, \tag{17}$$

where $n(m\Delta_\lambda)$ is the m^{th} sample of the total of M samples of refractive index within the corresponding resolution volume.

Data from the DH that corresponds to a radar resolution volume located at 2325 m are presented in FIG. 6 a, and the corresponding estimate of the 1-D refractive index spectra in Figure 6 b. The estimates clearly exhibit the -5/3 slope of the Kolmogorov turbulence spectra that confirms that the turbulence is in the inertial subrange, and C_n^2 estimates from the DH can be calculated directly by applying the methodology described in Sect. 2 (2.0.1).

Estimation of C_n^2 from the two instruments are presented in FIG. 7. Estimates from ascending and descending flights are presented in FIG. 7 a and FIG. 7 b respectively. In both figures, instantaneous C_n^2 estimated profiles obtained from the radar are presented in thin light gray lines, one every dwell time (12.5 seconds) over the time period corresponding to the co-located DH flight. All these radar estimates of C_n^2 have the segments of increased power from the DH reflections removed. The time

average of these radar instantaneous profiles at each altitude is presented in the thick dark gray line, exhibiting rather stationary gross features over this time period, but with significant variability in the details of the profiles over time. In contrast, the DataHawk measurements (red line) are not averaging over this 25 minute interval, but are instantaneous at a given altitude and time. So a more direct comparison would be obtained by extracting the radar returns at the altitude and time occupied by the DataHawk. As the DataHawk itself obliterates the radar returns there, due to is larger reflectivity, the next best comparison is to use an average of the radar returns just before and after the DataHawk reflection. This is presented by the thick blue line.

Turbulent layers are identified by a relative increase in the C_n^2 values at those altitudes. The agreement between the directly corresponding measurements (DH-red, SOUSY-blue) is remarkable, especially during the ascent portion of the morning flight, and above 2 km in the descent portion, where the radar data not only agree with the DH data in magnitude of C_n^2, but clearly follow each other in all the main layered features. Below 2 km on the descent the main variations become smaller, and the degree of detailed correspondence between the red and blue lines breaks down, although the averages over altitude continue to track well. The order of magnitude of C_n^2 profiles in this data correspond to intermediate to strong turbulence as defined in Doviak and Zrnić (1993).

4.2 Results from 10.7.2014, DH flight starting at 14:42:12

The afternoon DH flight was a balloon drop from an altitude of 6.7 km, several km south of the SOUSY radar. At approximately 4 km during the descent the DH arrived over the radar and started the helical descent at 2 m s^{-1}, continuing down to an altitude of 600 m before returning to the launch site. The calibrated radar returns during the flight are presented in FIG. 8. Note the small kink in the descent trajectory where the DH was inadvertently commanded to climb for a short period. Again the similarities in the altitudes of both trajectories (obtained from DH and detected by SOUSY) are excellent. As in the previous case, comparisons of C_n^2 were computed for both DH and SOUSY, and are presented in FIG. 9. For this case, there is only a descending flight over the radar, beginning at an altitude of $\sim$3.7 km. The location of the turbulent layers and their gross morphology are similar from both SOUSY and the DH data, except for the notable dip in the DH estimate of C_n^2 at 3.2 km. A closer inspection of FIG. 8 reveals some blue and white colored returns from the time just before the DH appearance at that altitude, but stronger returns afterward, indicating more variability at this altitude over time than throughout much of the flight. The averaged radar returns on either side of the DH location could cause a lack of correspondence if conditions are evolving at these faster time scales.

In each of the two cases above, the radar returns were calibrated by applying the appropriate calibration constant C to bring the DH and SOUSY C_n^2 estimates into general agreement. If this constant takes into account all the major factors, and the theory is adequate to describe the general conditions of interest, then this one constant should provide a correspondence that holds up over

time and over variations in conditions within those of interest. Finally, introducing the different parameters in Equation (13), the "best" value of the calibration constant C for the morning flight in the data shown above was 6×10^{-24} m$^{-5/2}$ mW^{-1} and 2×10^{-24} m$^{-5/2}$ mW^{-1} for the afternoon flight. The small discrepancies observed in the calibration constant for both flights might be caused by the change in the T/R switch which might have introduced a change in the sensitivity in the returned signal. After combining both (morning and afternoon) estimates, $C = 4 \times 10^{-24}$ m$^{-5/2}$ mW^{-1} was estimated for the whole day.

5 Conclusions and Future Work

Radar profiling of atmospheric turbulence and associated fine-structure has the potential to unravel important details of mixing and transport processes, owing to its instantaneous profiling capabilities near the boundary layer up into the stratosphere, and its ability to provide continuous measurements over extended periods. Unfortunately, radar return power is a complex function of difficult-to-measure radar parameters and various turbulent atmospheric scattering phenomena.

This paper showed how the measurement of the turbulent structure function of refractive index, and the associated parameter C_n^2 can be calibrated using a small unmanned aircraft system (the DataHawk) to provide coincident in-situ measurements inside the radar beam. This one-time calibration enables the radar to provide quantitative estimates of this turbulence parameter continuously thereafter, in turn enabling more detailed studies of these structures and their evolution.

Since turbulence can have a complex and evolving character, radar returns alone, by their dependence on refractive index alone, are not likely to suffice for study of turbulence processes in general, without information from other sources. Accordingly, future work will include periodic observational campaigns (every three months) that will include the DataHawk, SOUSY, and probably additional radars. These campaigns will seek to add estimates of the structure parameters of temperature C_T^2, turbulent energy dissipation rates ϵ, and horizontal winds. Another addition might be the recently installed Advanced Modular Incoherent Scatter Radar (AMISR) at JRO that operates at 450 MHz. AMISR has a pulse-to-pulse beam steer capability that could allow us to compare and validate horizontal winds estimates obtained from the DataHawk.

Acknowledgements. Thanks to all Jicamarca staff for their help with operation of SOUSY during this campaign, and especially to those that helped with the DataHawk balloon drop operations at JRO and the University of Colorado. This research is partially by NSF (1041963) and ARO (W911NF-12-2-0075) whose support is gratefully acknowledged. The Jicamarca Radio Observatory is a facility of the Instituto Geofisico del Peru operated with support from the NSF AGS-1433968 through Cornell University.

References

Alcantara, J. and Abad, R.: Sistema de Adquisición utilizando receptores digitales. Proyecto REX-2X, Informe técnico, Instituto Geofísico del Perú, 2008.

Balsley, B. B., Lawrence, D. A., Woodman, R. F., and Fritts, D. C.: Fine-scale characteristics of temperature, winds, and turbulence in the lower atmosphere (0 - 1300 m) over the south Peruvian coast, Boundary-Layer Meteor., pp. DOI 10.1007/s10 546–012–9774–x, 2012.

Bean, B. R. and Dutton, E. J.: Radio Meteorology, vol. 92 of *Natl. Bur. Stand. Monogr.*, Supt. Doc. U.S. Govt. Printing Office, Washington D.C., 1966.

Cohn, S. A.: Radar measurements of turbulent eddy dissipation rate in the troposphere: A comparison of techniques, J. Atmos. Oceanic Technol., 12, 85–95, 1995.

Doviak, R. J. and Zrnić, D. S.: Doppler Radar and Weather Observations, Academic Press, San Diego, CA, second edn., 1993.

Gossard, E. E. and Strauch, R. G.: Radar Observations of Clear Air and Clouds, Elsevier, 1983.

Hocking, W. K.: Measurement of turbulent eddy dissipation rates in the middle atmosphere by radar techniques: A review, Radio Sci., 20, 1403–1422, 1985.

Hocking, W. K.: An assessment of the capabilities and limitations of radars in measurements of upper atmospheric turbulence, Adv. Space Res., 17, 37–47, 1996.

Holdsworth, D. A. and Reid, I. M.: A simple model of atmospheric radar backscatter: Description and application to the full correlation analysis of spaced antenna data, Radio Sci., 30, 1263–1280, 1995.

Holton, J. R.: An Introduction to Dynamic Meteorology, vol. 88 of *International Geophysics Series*, Elsevier Academic Press, fourth edn., 2004.

Lawrence, D. A. and Balsley, B. B.: High-resolution atmospheric sensing of multiple atmospheric variables using the DataHawk small airborne measurement system, J. Atmos. Oceanic Technol., 30, 2352–2366. doi:10.1175/JTECH–D–12–00 089.1, 2013.

Luce, H., Fukao, S., Dalaudier, F., and Crochet, M.: Strong Mixing Events Observed near the Tropopause with the MU Radar and High-Resolution Balloon Techniques, J. Atmos. Sci., 59, 2885 – 2896, 2002.

Luce, H., Hassenpflug, G., Yamamoto, M., and Fukao, S.: Comparisons of refractive index gradient and stability profiles measured by balloons and the MU radar at a high vertical resolution in the lower stratosphere, Ann. Geophy., 25, 47–57, 2007.

Muschinski, A. P., Sullivan, P. P., Hill, R. J., Cohn, S. A., Lenschow, D. H., and Doviak, R. J.: First synthesis of wind-profiler signal on the basis of large-eddy simulation data, Radio Sci., 34, 1437–1459, 1999.

Ottersten, H.: Mean vertical gradient of potential refractive index in turbulent mixing and radar detection of CAT, Radio Sci., 4, 1247–1249, 1969.

Pope, S. B.: Turbulent Flows, Cambridge University Press, 2000.

Rogers, R. R. and Yau, M. K.: A short course in cloud physics, vol. 113 of *International series in natural philosophy*, Butterworth Heinemann, Burlington, MA, third edn., 1989.

Rüster, R., Klostermeyer, J., and Röttger, J.: SOUSY VHF radar measurements in the lower and middle atmosphere, IEEE Trans. Geosci. Remote Sens., GE-24, 966 – 974, 1986.

Scipión, D. E., Chilson, P. B., Fedorovich, E., and Palmer, R. D.: Evaluation of an LES-based Wind Profiler Simulator for Observations of a Daytime Atmospheric Convective Boundary Layer, J. Atmos. Oceanic Technol., 25, 1423–1436. DOI: 10.1175/2007JTECHA970.1, 2008.

Skolnik, M. I., ed.: Radar Handbook, McGraw-Hill, New York, second edn., 1990.

Stull, R.: Meteorology for Scientists and Engineers, Brooks/Cole Thomson Learning, second edn., 2000.

Tatarskii, V. I.: Wave Propagation in a Turbulent Medium, McGraw-Hill, New York, 1961.

Tatarskii, V. I.: The effects of turbulent atmosphere on wave propagation, NOAA U.S. Department of Commerce and NSF, 1971.

Wallace, J. M. and Hobbs, P. V.: Atmospheric science: An introductory survey, Elsevier Academic Press, second edn., 2006.

White, A. B.: Radar remote sensing of scalar and velocity microturbulence in the convective boundary layer, NOAA Technical Memorandum ERL ETL-276, Environmental Research Laboratories, 1997.

Woodman, R., Castillo, O., Michhue, G., Reyes, P., and Villegas, S.: SOUSY radar at Jicamarca: System Description, in: Extended Abstracts: 10^{th} International Workshop on Technical and Scientific Aspects of MST Radar, Piura, Peru, p. [Available online at http://jro.igp.gob.pe/mst10/CD/ExtAbs/Session5/I5_518.pdf], 2003.

Woodman, R., Michhue, G., Röttger, J., and Castillo, O.: The MPI-SOUSY-VHF radar at Jicamarca: High Altitude-Resolution Capabilities, in: Extended Abstracts: 11^{th} International Workshop on Technical and Scientific Aspects of MST Radar, Gadanki, India, p. [Available online at http://www.igp.gob.pe/descargas/ronw/SOUSY/The%20MPI%20Sousy%20Radar%20at%20Jicamarca%20extended%20abstract.pdf], 2007.

Woodman, R. F. and Guillen, A.: Radar observations of winds and turbulence in the stratosphere and mesosphere, J. Atmos. Sci., 31, 493–505, 1974.

Figure 1. The Jicamarca Radio Observatory (JRO) was the experimental site for the observational campaign. JRO is located approximately 25 km from the city of Lima. The DataHawk launch site is on the JRO property at 400 m from the main antenna (marked in yellow). The SOUSY radar is located next to the main antenna (marked in red). A picture of the SOUSY antenna elements is presented in the left-top corner of the dash rectangle.

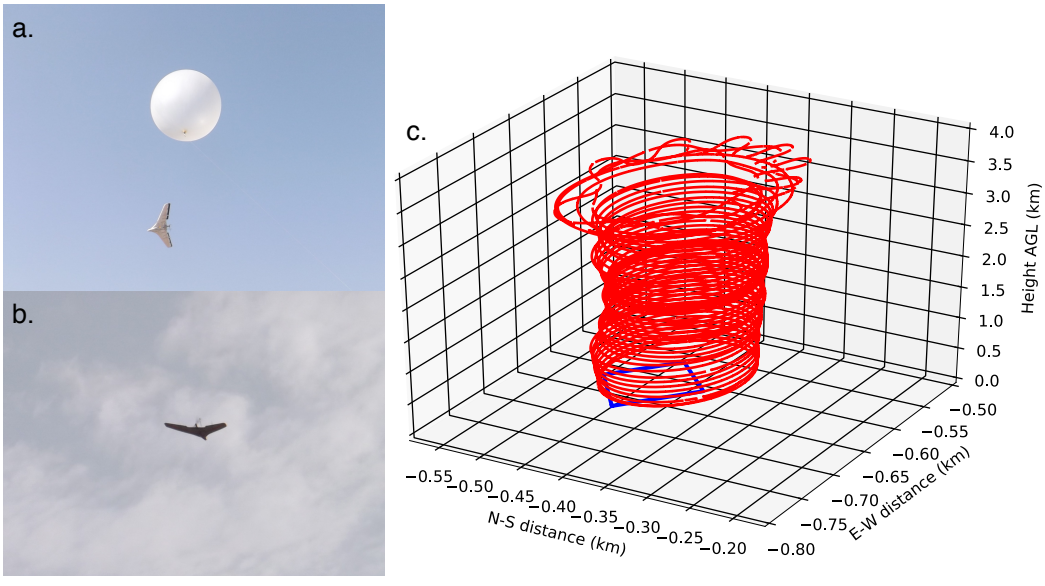

Figure 2. a. Balloon lifting the DataHawk for the afternoon data set on July 10^{th}, 2014. b. DataHawk flying towards the landing site for the same dataset at an approximate altitude of 50 m. c. Helical trajectory of the DataHawk descending from approximately 3.75 km to 500 m over the SOUSY radar (indicated in blue).

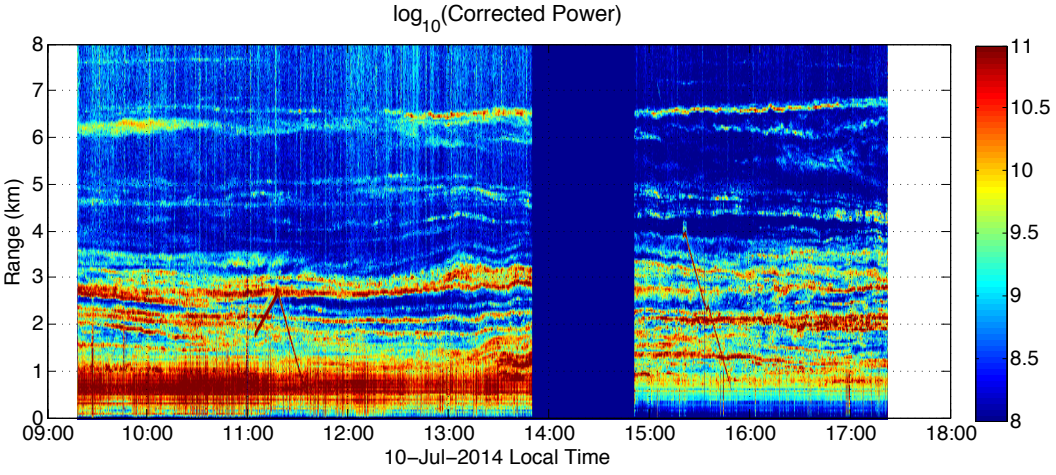

Figure 3. SOUSY daytime calibrated range-corrected received power for July 10^{th}, 2014 shows distinct turbulent layers from 500 m up to 7 km. The missing data between 14:00 and 15:00 were due to upgrades in the radar system that allowed for discrimination of echo returns bellow 1 km. DataHawk flights over the radar were easily detected as an increase of the radar returns between 11:05 to 11:30 and between 15:21 to 15:46.

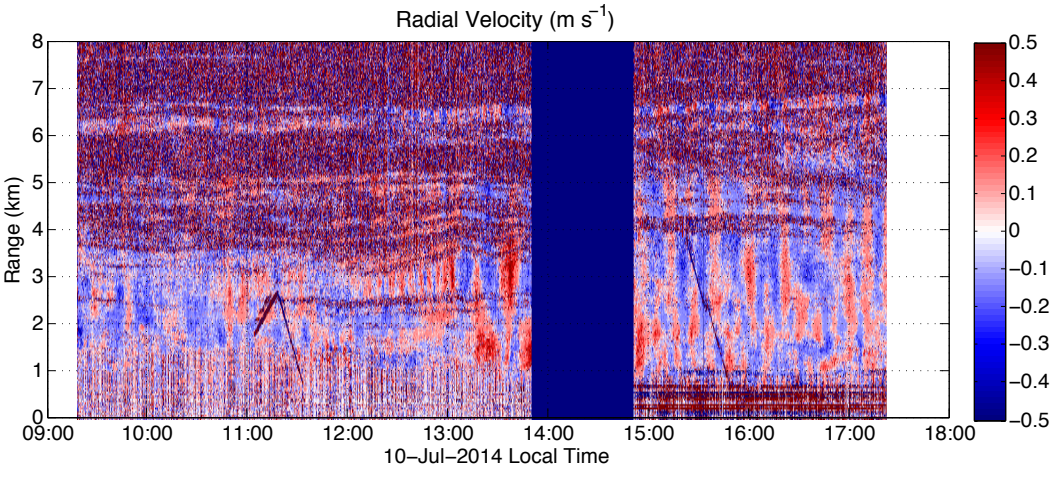

Figure 4. Daytime vertical velocity for July 10^{th}, 2014 shows stratified layers in the morning evolving into updrafts and downdrafts in the afternoon with a periodicity of approximately 10 minutes. The propagation of the updrafts reached altitudes close to 7 km.

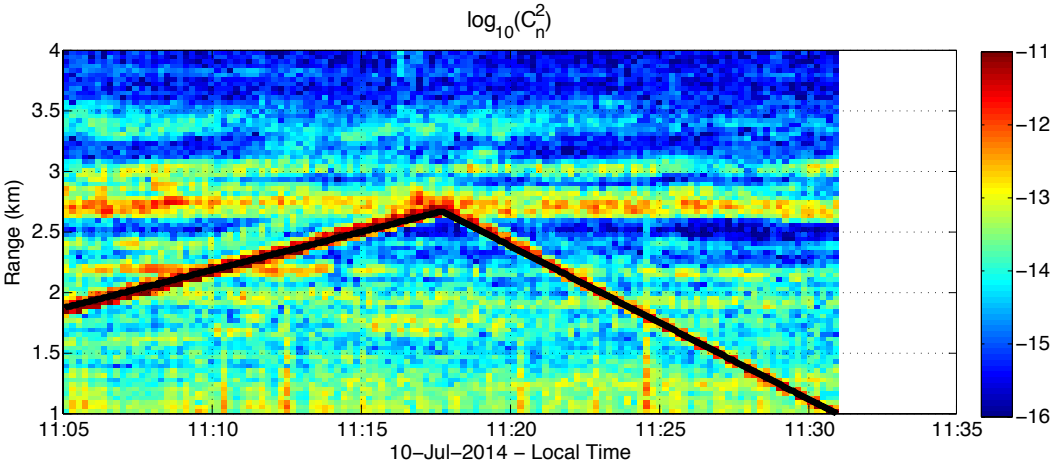

Figure 5. The black line represents the DataHawk altitude as a function of time plotted on top of the calibrated range corrected received power for the morning flight (11:05 - 11:30). The DataHawk was dropped by a tethered balloon at an approximate altitude of 2 km. In this case, there is an ascent from its initial altitude until 2.75 km, followed by a descent over SOUSY down to 1 km.

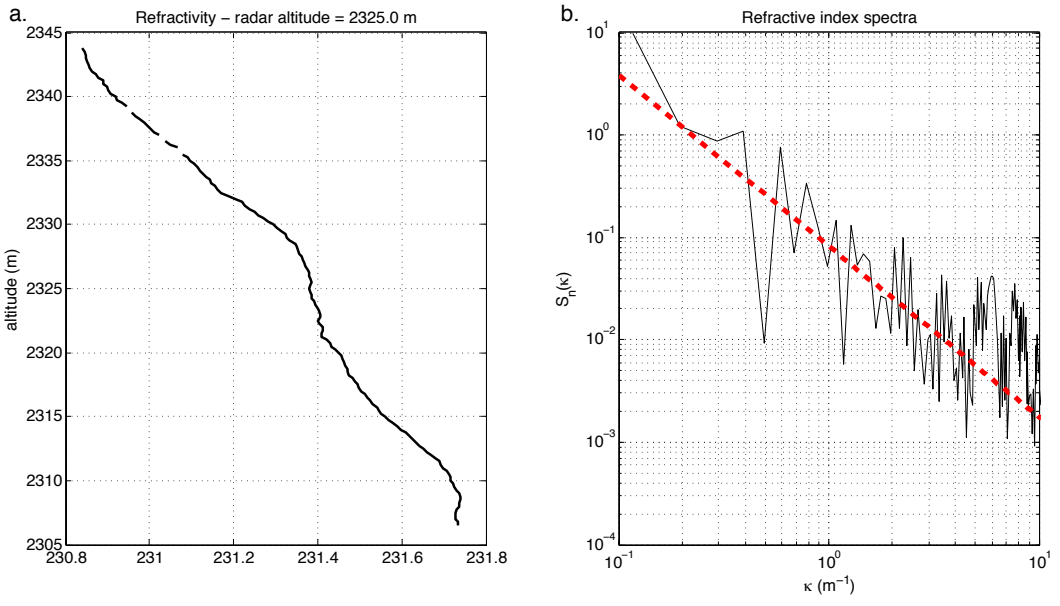

Figure 6. a. DataHawk refractivity resampled at a uniform spacing at 0.25 m during the ascent portion of the morning flight on July 7^{th}, 2014 for the corresponding radar resolution volume centered at 2.325 km. b. 1-dimensional refractive index spectra computed for the refractivity points in part a. presented on a logarithmic scale. The first-order curve fit clearly exhibits a -5/3 slope with wavenumber confirming that the data are in the inertial subrange.

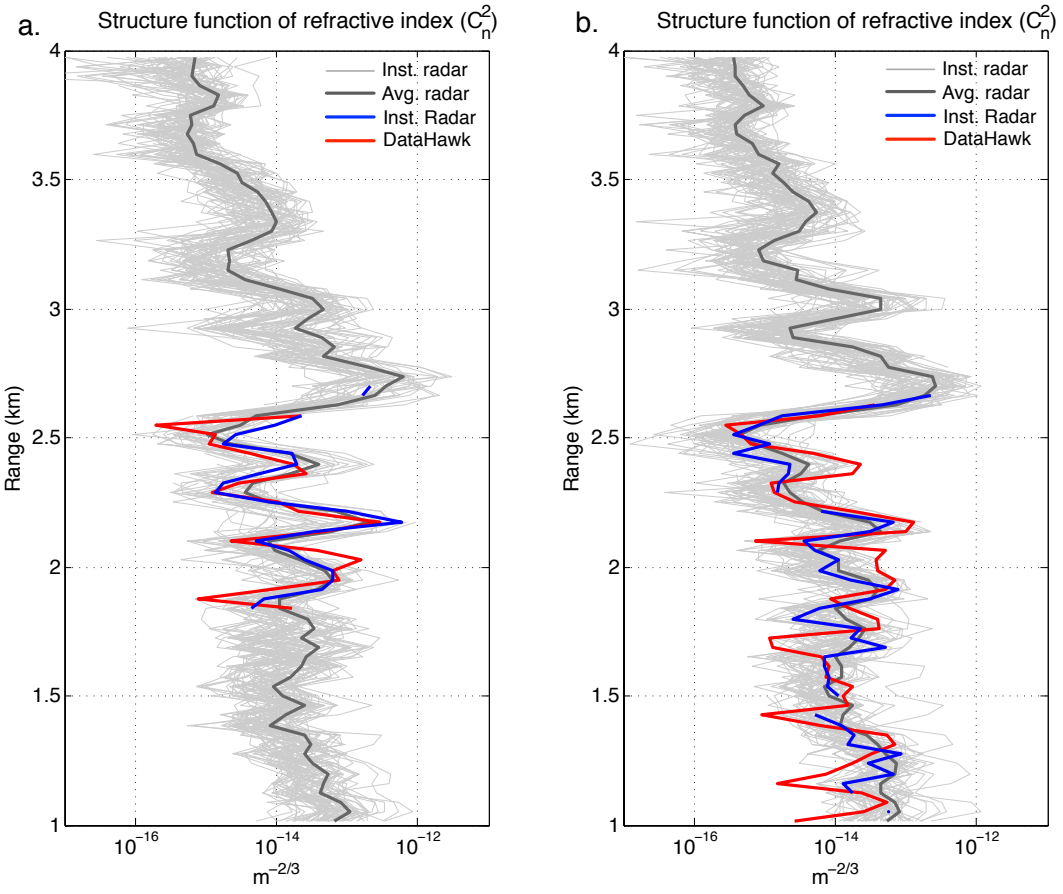

Figure 7. Structure parameter of refractive index obtained during the ascent (a.) and descent (b.) portions of the morning flight over the SOUSY radar. The light grey lines represent the multiple C_n^2 profiles obtained from SOUSY for the corresponding flight. The thick dark gray line is the radar average over the same period. The thick blue line represents the C_n^2 obtained from the radar around the closest time after the DH signature is removed. Finally, thick red line represents the C_n^2 obtained from the DataHawk.

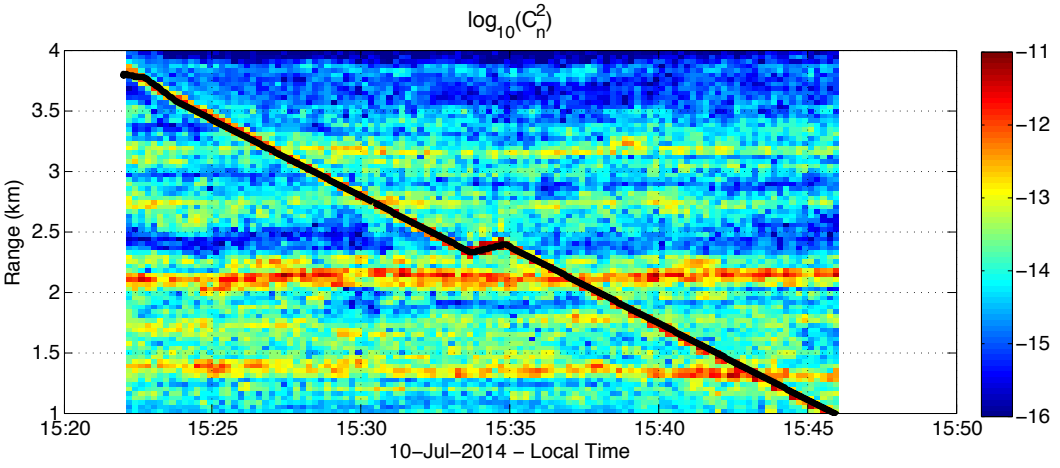

Figure 8. Similar to FIG. 5 but during the afternoon flight (15:21 - 15:46). In this case, the DataHawk was dropped by a “free" balloon at an altitude of approximately 7.5 km. However, due to the strong winds, the DataHawk was advected 4 km from the SOUSY radar, which caused 3 km drop during the time it took to regain its position over the radar.

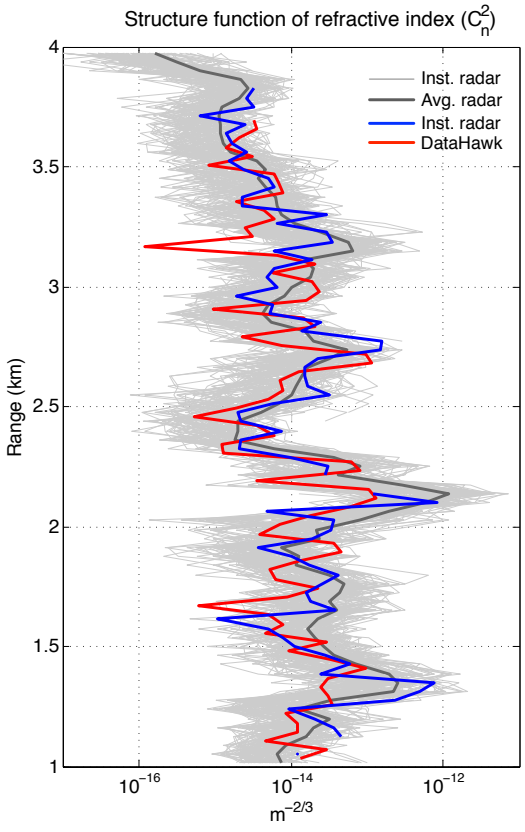

Figure 9. Similar to FIG. 7 but during the afternoon flight (15:21 - 15:46), which have only a descend portion.

Table 1. SOUSY Radar: Specifications

Quantity	Value
Radar type	Pulsed
Frequency	53.5 MHz
Wavelength	5.6 m
Beamwidth	$\sim$4.9°
Bandwidth	4 MHz
Transmitter peak power	20 kW
Receiver	Digital based on AD6620 chip
Processing type	Spectra
Number of FFT points	8
Number of coherent integrations	4096
Number of incoherent integrations	1
Dwell time	12.5 s
Unambiguos velocity	1.1 m s^{-1}
Mode 1	Characteristics
Inter pulse period (IPP)	57.2062 km
Pulse width	300 m
Code	Complementary 8-baud
Range resolution	37.5 m
Duty cycle	0.5244%
Mode 2	Characteristics
Inter pulse period (IPP)	57.2062 km
Pulse width	37.5 m
Code	None
Range resolution	37.5 m
Duty cycle	0.0655%

Table 2. DataHawk sensing system characteristics and capabilities (extracted from Lawrence and Balsley (2013)).

	Value		Value
Wingspam	1 m	Alt. (balloon drop)	>9 km MSL
Mass	0.7 kg	Alt. (bungee launch)	>2 km AGL
Design	Flying wing, rear propeller	Turning radius	>50 m
Telemetry	IEEE 802.15.4 at 2.4 GHz	Climb rate	<5 m s^{-1}
Propulsion	Electric motor, folding propeller	Downlink throughput	>1500 bytes s^{-1}
Autopilot	CU custom design (CUPIC)	Downlink update rate	10 Hz
Control	Auto-Helix, Balloon-Drop	Sensor Sampling	>100 Hz
Power	11-V LiPo battery, 2600 mA h^{-1}	Data storage (on board)	16 MB

Sensing capabilities

Type	Resolution	Accuracy; range	Time const.; cadence	Notes
Location (GPS)	0.1 m	10 m; worldwide	1 s; 4 Hz	Real time
In-situ temperature	0.1°C	2°C; -60° to +40°	5 s; 8.1 Hz	Real time
Relative humidity	0.01%	2%; 0% – 100%	5 s; 8.1 Hz	Real time
Cold-wire temperature	<0.003°C	2°C; -60°C to +40°C	0.5 ms; 81 Hz	Real time; postflight calibration
Airspeed	0.01 m s^{-1}	0.2 m s^{-1}; 0 – 30 m s^{-1}	0.3 ms; 81 Hz	Real time

Table 3. SOUSY and DataHawk coordinated events

Date	Period	Max. Altitude	Radar Mode
July 10^{th}, 2014	11:05 – 11:30 UTC-5	2800 m	Mode 2
July 10^{th}, 2014	15:21 – 15:46 UTC-5	3850 m	Mode 1